Remote local photoactivation of morphine produces analgesia without opioid-related adverse effects

Marc López-cano, Joan Font, Ester Aso, Kristoffer Sahlholm, Gisela Cabré, Jesús Giraldo, Yves de Koninck, Jordi Hernando, Amadeu Llebaria, Víctor Fernández-dueñas, et al.

Received: 7 January 2021 | Revised: 19 July 2021 | Accepted: 23 July 2021

DOI: 10.1111/bph.15645

THEMED ISSUE ARTICLE

Remote local photoactivation of morphine produces analgesia without opioid-related adverse effects

Marc López-Cano[1,2] | Joan Font[3,4] | Ester Aso[1,2] | Kristoffer Sahlholm[1,2,5,6] | Gisela Cabré[7] | Jesús Giraldo[8,9,10] | Yves De Koninck[11,12] | Jordi Hernando[7] | Amadeu Llebaria[3] | Víctor Fernández-Dueñas[1,2] | Francisco Ciruela[1,2]

[1]Pharmacology Unit, Department of Pathology and Experimental Therapeutics, School of Medicine and Health Sciences, Institute of Neurosciences, University of Barcelona, L'Hospitalet de Llobregat, Barcelona, Spain

[2]Neuropharmacology & Pain Group, Neuroscience Program, Bellvitge Institute for Biomedical Research, IDIBELL, L'Hospitalet de Llobregat, Barcelona, Spain

[3]MCS, Laboratory of Medicinal Chemistry, Institute for Advanced Chemistry of Catalonia (IQAC-CSIC), Barcelona, Spain

[4]Institut de Génomique Fonctionnelle (IGF), University of Montpellier, CNRS, INSERM, Montpellier, France

[5]Department of Neuroscience, Karolinska Institutet, Stockholm, Sweden

[6]Department of Integrative Medical Biology, Umeå University, Umeå, Sweden

[7]Departament de Química, Universitat Autònoma de Barcelona, Cerdanyola del Vallès, Spain

[8]Laboratory of Molecular Neuropharmacology and Bioinformatics, Unitat de Bioestadística and Institut de Neurociències, Universitat Autònoma de Barcelona, Bellaterra, Spain

[9]Unitat de Neurociència Traslacional, Parc Taulí Hospital Universitari, Institut d'Investigació i Innovació Parc Taulí (I3PT), Institut de Neurociències, Universitat Autònoma de Barcelona, Barcelona, Spain

[10]Instituto de Salud Carlos III, Centro de Investigación Biomédica en Red de Salud Mental, CIBERSAM, Barcelona, Spain

[11]Institut Universitaire en Santé Mentale de Québec, Québec, Quebec, Canada

[12]Department of Psychiatry and Neuroscience, Université Laval, Québec, Quebec, Canada

Correspondence
Francisco Ciruela and Víctor Fernández-Dueñas, Pharmacology Unit, Department of Pathology and Experimental Therapeutics, School of Medicine and Health Sciences, Institute of Neurosciences, University of Barcelona, L'Hospitalet de Llobregat, Barcelona, Spain.
Email: fciruela@ub.edu; vfernandez@ub.edu

Amadeu Llebaria, MCS, Laboratory of Medicinal Chemistry, Institute for Advanced Chemistry of Catalonia (IQAC-CSIC), Barcelona, Spain.
Email: amadeu.llebaria@iqac.csic.es

Background and Purpose: Opioid-based drugs are the gold standard medicines for pain relief. However, tolerance and several side effects (i.e. constipation and dependence) may occur upon chronic opioid administration. Photopharmacology is a promising approach to improve the benefit/risk profiles of these drugs. Thus, opioids can be locally activated with high spatiotemporal resolution, potentially minimizing systemic-mediated adverse effects. Here, we aimed at developing a morphine photoderivative (photocaged morphine), which can be activated upon light irradiation both *in vitro* and *in vivo*.

Experimental Approach: Light-dependent activity of pc-morphine was assessed in cell-based assays (intracellular calcium accumulation and electrophysiology) and in mice (formalin animal model of pain). In addition, tolerance, constipation and dependence were investigated *in vivo* using experimental paradigms.

Key results: In mice, pc-morphine was able to elicit antinociceptive effects, both using external light-irradiation (hind paw) and spinal cord implanted fibre-optics. In

Abbreviations: CPP, conditioned place preference; DRG, dorsal rood ganglion; GIRK, G protein-coupled inwardly rectifying potassium channel; PC-morphine, photocaged-morphine.

Funding information
Instituto de Salud Carlos III, Grant/Award Number: PIE14/00034; Catalan government, Grant/Award Numbers: 2017 SGR 465, 2017 SGR 1604; FEDER/Ministerio de Ciencia, Innovación y Universidades-Agencia Estatal de Investigación, Grant/Award Numbers: CTQ2017-89222-R, SAF2017-87199-R, SAF2017-87349-R

addition, remote morphine photoactivation was devoid of common systemic opioid-related undesired effects, namely, constipation, tolerance to the analgesic effects, rewarding effects and naloxone-induced withdrawal.

Conclusion and Implications: Light-dependent opioid-based drugs may allow effective analgesia without the occurrence of tolerance or the associated and severe opioid-related undesired effects.

KEYWORDS
dependence, morphine, pain, photopharmacology, tolerance

1 | INTRODUCTION

Pain is a multidimensional pathological condition that diminishes the quality of life of patients, interfering in their daily family and work activities. Different epidemiological studies conclude that, at present, the prevalence of chronic pain is very high, with at least 20% of the population being affected (Blyth et al., 2004; Cousins & Lynch, 2011). This is the reason why analgesics are among the most-consumed drugs (Urquhart, 2018). Importantly, the choice for analgesic medications is currently based on the World Health Organization (WHO) analgesic three-step ladder (Vargas-Schaffer & Cogan, 2014). This ladder classifies drugs according to their analgesic potency and suggests a progressive use (from less to more potent drugs) depending on the needs. On the top step of the WHO ladder, as the most effective drugs for pain relief, we mainly find the so-called major opioids (**morphine**, **methadone**, **hydromorphone**, **oxycodone**, oxycodone/**naloxone**, **fentanyl**, **buprenorphine** and **tapentadol**) (Law & Loh, 2013; McDonald & Lambert, 2016).

Major opioids exhibit important and severe side effects (i.e. respiratory depression, constipation, dependence, hyperalgesia and neurotoxicity) and patients might develop tolerance to their analgesic effects, which can limit their use (Law & Loh, 2013; McNicol et al., 2003; Volkow & Thomas McLellan, 2016). These drugs have been classically held in reserve for a limited number of conditions (i.e. cancer-related pain). In recent years, however, opioid use has increased exponentially (Cheung et al., 2014; Nuckols et al., 2014). Epidemiological data indicate that a more careful approach should be taken when using opioids regularly (McNicol et al., 2003). In the ongoing opioid epidemic in the United States, more than 100 people die every day from opioid overdosing (Kolodny et al., 2015). In line with this, ~30% of patients prescribed with opioids do not use them properly, and ~10% of patients develop dependence (Kolodny et al., 2015).

Altogether, it seems clear that finding novel strategies to reduce tolerance, which counteracts analgesic efficacy and drives dose escalation, and opioid-related side effects should be a major goal in analgesic research. One of the most exciting approaches to reduce off-target effects mediated by systemic drug administration is photopharmacology (Lerch et al., 2016; Velema et al., 2014).

What is already known

- Prescribing opioid medications for pain relief exposes people to the risk of opioid use disorders.
- Safe, effective, and non-addictive strategies to manage pain urge to be explored.

What does this study add

- We apply a novel pharmacological approach based on the use of light controlling opioid activity, photocaged morphine.
- Photocaged morphine has high spatiotemporal resolution and reduced side effects.

What is the clinical significance

- This novel light-based approach may provide an optimal benefit/risk ratio for opioid-based therapies.

Photopharmacology is a new discipline that allows for the temporal and spatial remote control of ligand activity specifically in the target tissues of select pharmacological compounds (Lerch et al., 2016; Velema et al., 2014). Recently, we developed a photosensitive negative allosteric modulator of the **metabotropic glutamate type 5 receptor** ($mGlu_5$ receptor), which elicited analgesic effects upon peripheral and central irradiation (Font et al., 2017). Based on this experience, here we aimed to design, synthesize and characterize a photosensitive morphine derivative allowing the local light-dependent release of morphine to minimize the appearance of analgesic tolerance and opioid-related side-effects. Indeed, we managed to photodeliver morphine to the spinal cord by means of flexible fibre-optics (Bonin et al., 2016), which could represent a highly translational strategy. Overall, the novel light-based approach presented here may represent a proof of concept model for the safe use of opioid drugs in clinical settings.

2 | METHODS

2.1 | Drug synthesis

All the chemicals and solvents were provided from commercial suppliers and used without purification, except the anhydrous solvents, which were treated previously through a system of solvent purification (*PureSolv*), degasified with inert gases and dried over alumina or molecular sieves (dimethyl formamide).

2.1.1 | Synthesis of 4-(bromomethyl)-7-(diethylamino)-*2H*-chromen-2-one

A solution of 7-(diethylamino)-4-(hydroxymethyl)coumarin (DEACM) (358 mg, 1.45 mmol) and triethylamine (0.40 ml, 2.9 mmol) in DCM (12 ml) was cooled to 0°C, methanesulfonyl chloride (0.17 ml, 2.1 mmol) was added dropwise, and the reaction mixture was stirred 2 h at 0°C. The mixture was quenched with cold saturated $NaHCO_3$ (50 ml), and DCM (20 ml) was added. The organic layer was separated, washed with brine (2 × 50 ml), dried over Na_2SO4, filtered off and concentrated under reduced pressure. Afterwards, the crude was solved in THF (12 ml), and LiBr (503 mg, 5.8 mmol) was added. The reaction mixture was stirred for 2.5 h. The mixture was concentrated, DCM (30 ml) was added, washed with brine (2 × 30 ml), dried over Na_2SO_4 and the solvent removed under reduced pressure. The crude was purified through flash silica column chromatography using DCM/AcOEt 99:1 as mobile phase, affording the title compound (140) (200 mg, 44%) as a yellow solid (Seven et al., 2014). ^{1}H-NMR (400 MHz, Chloroform-d) δ 7.49 (d, $J = 9.0$ Hz, 1H), 6.62 (dd, $J = 9.0$, 2.6 Hz, 1H), 6.51 (d, $J = 2.6$ Hz, 1H), 6.13 (s, 1H), 4.40 (d, $J = 0.7$ Hz, 2H), 3.42 (q, $J = 7.1$ Hz, 4H), 1.21 (t, $J = 7.1$ Hz, 6H).

2.1.2 | Synthesis of 7-(diethylamino)-4-((((4*R*,7*S*,12b*S*)-7-hydroxy-3-methyl-2,3,4,4*a*,7,7*a*-hexahydro-1*H*-4,12-methanobenzofuro[3,2-*e*]isoquinolin-9-yl)oxy)methyl)-2*H*-chromen-2-one hydrochloride (photocaged-morphine).

To a solution of (4*R*,7*S*,12b*S*)-3-methyl-2,3,4,4*a*,7,7*a*-hexahydro-1*H*-4,12-methanobenzofuro[3,2-*e*]isoquinoline-7,9-diolhydrochloride (morphine hydrochloride) (250 mg, 0.87 mmol) in DMF (7 ml) was added K_2CO_3 (266 mg, 1.93 mmol), and the mixture was stirred 15 min. After this time, a solution of 4-(bromomethyl)-7-(diethylamino)-2*H*-chromen-2-one (299 mg, 0.96 mmol) in DMF (2 ml) was added to the reaction mixture and stirred 4 days at room temperature in the dark. Afterwards, AcOEt (50 ml) was added. Then, the mixture was washed with a saturated solution of $NaHCO_3$ (3 × 50 ml), brine (3 × 50 ml), dried over Na_2SO_4, filtered off and the solvent removed under vacuum. The brown crude solid was purified through *flash* silica column chromatography using DCM/MeOH 94:6 as mobile phase. The fluorescent-yellow oil was solved in 7 ml of ether, and HCl in dioxane (4N) was added dropwise. The precipitate was collected by filtration and washed several times with ether, to afford the title compound (215 mg, 47%) as a yellow solid. This compound is light sensitive and should be maintained and manipulated protected from illumination. Mp: 301–303°C. ^{1}H-NMR (400 MHz, DMSO-d_6) δ 7.57 (d, $J = 9.0$ Hz, 1H), 6.83 (d, $J = 8.2$ Hz, 1H), 6.71 (dd, $J = 9.1$, 2.5 Hz, 1H), 6.58 (d, $J = 8.3$ Hz, 1H), 6.55 (d, $J = 2.5$ Hz, 1H), 6.14 (s, 1H), 5.73–5.66 (m, 1H), 5.33 (s, 2H), 5.30–5.26 (m, 1H), 4.18 (dq, $J = 5.7$, 2.7 Hz, 1H), 4.12 (d, $J = 6.9$ Hz, 1H), 3.57 (s, 3H), 3.44 (q, 4H), 3.30–3.17 (m, 2H), 3.08 (s, 1H), 3.02 (d, $J = 5.0$ Hz, 1H), 2.85 (d, $J = 4.7$ Hz, 2H), 2.81–2.72 (m, 1H), 2.36–2.26 (m, 1H), 1.19 (t, $J = 7.1$ Hz, 6H). ^{13}C-NMR (101 MHz, DMSO-d_6) δ 160.76, 155.78, 151.57, 147.67, 139.92, 134.89, 129.81, 125.78, 125.38, 125.09, 119.34, 116.79, 105.63, 91.08, 66.73, 65.84, 59.33, 46.14, 44.10, 42.47, 41.36, 40.40, 37.52, 32.45, 21.05, 12.29. HPLC-PDA-MS (using method A) RT: 2.59 min, $\lambda_{max} = 214$, 246, 317, 389 nm; purity > 98% (254 nm). HRMS (m/z): $[M + H]^+$ calcd. For $C_{31}H_{34}N_2O_5$, 515.2546; found, 515.2537.

2.2 | Photochemical characterization

To investigate the uncaging process of photocaged-morphine a 7 μM solution of this compound in phosphate-buffered saline (PBS):DMSO 99:1 was irradiated at 405 nm and 0.56 $W{\cdot}cm^{-2}$ using a cw laser (MDL-E-405, Scitec Instruments Ltd., Wiltshire, UK). The changes in UV–vis absorption were monitored in time using an HP 8453 spectrophotometer (Agilent Technologies, Inc., Colorado Springs, CO, USA). An aliquot of the irradiated sample after 120 min was analysed by MS (ESIMS) in a micrOTOF-Q spectrometer (Bruker Corporation, Billerica, MA, USA) (Figure S1). Control experiments were conducted by irradiating morphine and DEACM (Indofine Chemical Co., Hillsborough, NJ) solutions at the same conditions. From the UV–vis absorption measurements, the photouncaging quantum yield of photocaged-morphine was determined, as previously described (Lees, 1996), with the photoisomerization process of the closed state of 1,2-bis(5-chloro-2-methyl-3-thienyl)perfluorocyclopentene in hexane at 405 nm as a reference ($\Phi_{iso} = 0.13$) (Higashiguchi et al., 2005).

2.3 | Cell culture

HEK-293T cells (RRID:CVCL_0063), permanently expressing **μ-opioid receptors** were used (kindly provided by Laboratorios Dr. Esteve, Barcelona, Spain). Cells were grown by seeding them in a 96-well plate (10,000 cells per well) using DMEM (Sigma-Aldrich, St. Louis, MO, USA) supplemented with 100 $U{\cdot}ml^{-1}$ penicillin (Biowest, Nuaillé, France), 100 $mg{\cdot}ml^{-1}$ streptomycin (Biowest), 10% v/v FBS (Invitrogen, Carlsbad, CA, USA), 1 mM pyruvic acid (Biowest), non-essential amino acids (Biowest) and 2 mM L-glutamine (Biowest) in the presence of 0.1 $mg{\cdot}m^{-1}$ geneticin (InvivoGen, Tolouse, France). Cells

were kept at 5% CO_2, 37°C, and 95% humidity conditions. Cells were tested for mycoplasma content; thus, only mycoplasma-free cells were used.

2.4 | Dorsal rood ganglion (DRG) isolation and primary culture

DRG from adult male and female CD-1 mice was extracted as previously described (Tulleuda et al., 2011). In brief, animals were killed by cervical dislocation preceded by anaesthesia before the thoracic cavity was exposed, and the viscera removed to access to the vertebras before performing a laminectomy. Sensory ganglia (containing DRGs) were dissected, cleaned and maintained in ice-cold Mg^{2+}/Ca^{2+} free-PBS (Sigma-Aldrich) supplemented with glucose (10 mM), HEPES (10 mM), penicillin (100 UI·ml^{-1}) and streptomycin (100 μg·ml^{-1}) until dissociation. Subsequently, sensory ganglia were chemically dissociated in 2 ml of HAM's F-12 (Biowest) containing collagenase type IA (1 mg·ml^{-1}; Sigma-Aldrich) and BSA (1 mg·ml^{-1}; Sigma-Aldrich) for 1 h and 45 min at 37°C. Afterwards, ganglia were centrifuged at 100× *g* for 5 min. The pellet was resuspended with 1 ml of trypLE express (Gibco, Carlsbad, CA, USA) in supplemented PBS for 15 min at 37°C. Ganglia were collected by centrifugation at 100× *g* for 5 min and resuspended in 2 ml of supplemented DMEM. Finally, ganglia were mechanically disaggregated by forcing them to pass through a fire-polished Pasteur pipette until no cell aggregates were observed. DRG neurons were plated onto poly-L-lysine and laminin-coated 96-well plates with supplemented Dulbecco's Modified Eagle Medium (DMEM).

2.5 | Intracellular calcium determinations

Intracellular calcium determinations were performed using Fluo-4 NW Calcium Assay Kit (ThermoFisher Scientific, Waltham, MA, USA) as previously described (Font et al., 2017). In brief, HEK-293T cells permanently expressing μ receptors or DRGs neurons grown in 96-well black plates were incubated with Fluo4 NW following manufacturer's indications. Subsequently, cells were treated with vehicle (HBSS), morphine or photocaged-morphine maintained in dark or previously irradiated for 15 min at 405 nm (1 Hz frequency, 500 ms pulses and 2000 mA intensity LED and 23 mW output power). Fluo4 NW emission (i.e. 535 nm) was recorded in real-time upon 485 nm excitation in a POLARstar Omega multi-mode microplate reader (BMG Labtech GmbH, Ortenberg, Germany). The results were expressed as the percentage of μ receptor activation induced by treatments following the equation:

$$Ca^{2+}\text{accumulation}\,(\%) = \left[\left(AUC^{veh} - AUC^{drug}\right)/AUC^{veh}\right] \times 100$$

where AUC^{veh} and AUC^{drug} represent the AUC value in the vehicle- and drug-treated conditions, respectively.

2.6 | Electrophysiology

HEK-293T cells stably expressing μ receptors were cultured as described above. Cells were seeded into six-well plates (300,000 cells per well) and transiently transfected the following day with cDNA (in μg per well) encoding **G protein-coupled inwardly rectifying potassium channel type 1 (K_{ir}3.1;GIRK1)**-YFP (1.5) and **K_{ir}3.2 (GIRK2)** (1.5) using polyethylenimine (PEI, linear, 25 kDa; Polysciences Europe GmbH, Hirschberg an der Bergstrasse, Germany) (Longo et al., 2013). Twenty-four hours after transfection, cells were lifted off using Versene (Gibco), diluted ~1/5 and re-seeded onto 18-mm glass coverslips (VWR International Eurolab, Llinars del Vallès, Spain) coated with poly-L-ornithine (Sigma–Aldrich), and kept in culture for additional 2–4 days prior to experiments. Subsequently, coverslips were mounted in an Attofluor holder and placed at an inverted Axio Observer microscope (Zeiss, Oberkochen, Germany) equipped with a 63× oil-immersion objective. A Polychrome V (Till Photonics GmbH, Gräfelfing, Germany) was used as light source for fluorescence excitation. The extracellular high-potassium buffer contained (in mM): 113 NaCl, 0.34 Na_2HPO_4, 25 KCl, 0.44 KH_2PO_4, 0.5 $MgCl_2$, 0.4 Mg_2SO_4, 1.26 $CaCl_2$, 10 HEPES, 2 D-glucose and 1 ascorbic acid; pH 7.4 with NaOH.

Single cells were selected for recording based on their plasma membrane expression of the tagged GIRK1-YFP protein, as judged by their fluorescence (Figure 3c). Cells selected for recording were voltage-clamped in the whole-cell configuration using an Axopatch 200B amplifier (Molecular Devices, Sunnyvale, CA, USA). A Digidata 1440 analogue/digital converter (Molecular Devices) was used for interfacing the amplifier with a personal computer. Patch micropipettes were pulled from borosilicate glass capillaries (GC120F-10, Harvard Apparatus, Edenbridge, UK) to have a resistance of 4–10 MΩ when filled with intracellular solution [in mM; 10 NaCl, 120 KCl, 5 $MgCl_2$, 1 EGTA, 5 HEPES, 5 ATP, 0.2 GTP (pH 7.2 with NaOH)]. Cells were voltage-clamped at −80 mV, and test compounds were applied using a pressure-driven, computer-controlled perfusion system (Octaflow; ALA Scientific Instruments Inc., Westbury, NY, USA). Increases in inward current were used as readout of μ receptor activation. During each recording, cells were first exposed to a saturating concentration (10 μM) of morphine, in order to evoke a control response against which the subsequent responses could be normalized. Increasing concentrations (10 nM to 10 μM) of morphine, or the uncaged (1 Hz frequency, 500 ms pulses and 2000 mA intensity LED and 23 mW output power) or caged derivative (pc-Mor), were then applied consecutively, each application lasting 20 s. Experiments were carried out at room temperature.

2.7 | Animals

Adult male and female CD-1 mice (RRID:MGI:2686808; animal facility of University of Barcelona) weighing 20–25 g were used and randomly assigned to each experimental group. The University of

Barcelona Committee on Animal Use and Care approved the protocol (number: 10034). Following the approved experimental protocol, all animals were supervised daily to assess signs of adverse effects during treatment. A retrospective analysis of the protocol demonstrated that no corrective measures (i.e. use of analgesics) were needed. Animals were housed and tested in compliance with the guidelines provided by the Guide for the Care and Use of Laboratory Animals (Clark et al., 1997) and following the European Union directives (2010/63/EU). Mice were housed in groups of five in standard cages with ad libitum access to food and water and maintained under a non-reversed 12 h dark/light cycle (starting light period at 7:30 AM), 22°C temperature, and 66% humidity (standard conditions). All animal experimentation was carried out in a period comprehended between 9:00 AM to 6:00 PM by a researcher blind to drug treatments. Animal studies are reported in compliance with the ARRIVE guidelines (Percie du Sert et al., 2020) and with the recommendations made by the *British Journal of Pharmacology* (Lilley et al., 2020).

2.8 | Epidural fibre-optic implantation

Both epidural fibre-optics production and implantation surgery were performed as previously described (Bonin et al., 2016). In brief, a length of multimode plastic fibre (240 μm core, 250 μm diameter with cladding, 0.63 NA) modified with a diffusive tip to enable multidirectional diffusion of light from the fibre was used to manufacture the epidural fibre-optic implant (MMF_POF_240/250-0.63_8cm_DLF; Doric Lenses, Quebec, Canada). The fibre was fitted with a stainless ferrule (2.5 mm diameter, 270 μm bore; Thor Labs, Bergkirchen, Germany) using epoxy blue-dye (Fosco, Pleasanton, CA, USA). The length of the fibre from the end of the ferrule to the diffusive tip was 40 mm for 20–25 g adult CD-1 mice. A base of dental cement (Agnthos, Lidingö, Sweden) was added to the ferrule prior to implantation to facilitate fixation on the skull of the mouse. Mice were anaesthetized with a combination of ketamine/xylacine (dose of 100 $mg{\cdot}kg^{-1}$ body weight for ketamine and 10 $mg{\cdot}kg^{-1}$ for xylacine) animals, spontaneously breathing, were keep on a heated blanket before the epidural fibre implantation surgery was performed as described (Bonin et al., 2016). Thus, the fibre-optic was carefully inserted through the atlanto-occipital membrane and under the first vertebrae (C1), immediately rostral to C1, with the head held at an acute, downward angle. The correct positioning of the fibre tip near L1 (corresponding to spinal segments L4-L6) was confirmed by connecting the fibre to the LED-based light source and observing the illuminated region on the back. Finally, once the fibre was correctly positioned, the dental cement base of the fibre was fixed to the skull with Loctite 454 Prism instant adhesive and the incision sutured. The fibre-optic implanted mice were let to recover from anaesthesia and supervised to ensure lack of paralysis for 1 week. After recovery, animals looked healthy. However, mice presenting any movement abnormality (less than 10% of total number surgeries performed) were automatically excluded.

2.9 | Formalin test

The formalin animal model of pain was performed as previously described (López-Cano et al., 2019). In brief, mice ($n = 5–6$ per group) were administered intraperitoneally (i.p.) with vehicle, morphine or photocaged-morphine 35 min before a diluted formalin solution (20 μl of 2.5% formalin/0.92% formaldehyde; Sigma-Aldrich) was intraplantarly (i.pl.) injected in the mid-plantar surface of the right hind paw of the mouse. The formalin-induced nociceptive behaviour in light or mock manipulated (dark) conditions was quantified as the time spent licking or biting the injected paw during the 35 min after the injection of formalin. The initial acute phase (0–5 min; phase I), was followed by a relatively short quiescent period (15 min), which was then followed by a prolonged response (20–35 min; phase II). For the peripheral photocaged-morphineuncaging, the hind paw was directly irradiated with a LED-based fibre-optic system (Doric Lenses Inc.) at 405 nm light (or dark) for 15 min before the recording of each phase. The present interval was selected according to preliminary pilot experiments (Figure S2) showing non-optimal photo-uncaging reliable processes for periods less than 15 min. We did not test larger irradiation times (i.e. more than 15 min), since phase II licking/biting determinations in the formalin injected paw would have been interfered (Figure 5a). Nevertheless, a 15-min irradiation of photocaged-morphine produced a significant antinociceptive effect in both formalin test phases (Figure S2). To uncage photocaged-morphine at the lumbar segment (L4–L6) of the spinal cord, mice were irradiated through the epidural implanted flexible fibre-optic (Doric Lenses Inc.) with 405 nm light (or dark) for 15 min before the recording of each phase. The 405 nm light pulses lasted 500 ms each and were administered at 1 Hz frequency with 23 mW output power and 2000 mA intensity. Antinociception induced by the different treatments was calculated with the equation:

$$\text{Antinociceptive effect}\,(\%) = [(\text{LTV} - \text{LTD})/\text{LTV}] \times 100$$

where LTV and LTD represent the licking/biting time in the vehicle- and drug-treated animals, respectively.

2.10 | Gastrointestinal transit

Gastrointestinal transit (GIT) studies were performed to assess the constipation level caused by opioid treatment. Briefly, 6 h prior to the gastrointestinal transit experimental procedure, mice were individually housed and fasted. Food was restricted but animal had free access to water for the entire study. Afterwards, mice were intragastrically administered with 0.25 ml of a suspension of 10% vegetable charcoal Norit A® (Sigma-Aldrich) in 5% gum acacia (Sigma-Aldrich) plus vehicle, morphine (10 $mg{\cdot}kg^{-1}$, i.p.) or photocaged-morphine(10 $mg{\cdot}kg^{-1}$, i.p.). Immediately, the hind paw was directly irradiated with a LED-based fibre-optic system (Doric Lenses Inc.) at 405 nm light or mock manipulated (dark). The 405 nm light regime consisted of pulses that lasted 500 ms each and were

administered at 1 Hz frequency with 23 mW output power and 2000 mA intensity for 15 min. Twenty minutes later, mice were killed, and the stomach and small intestine dissected to collect the intestinal segment between the stomach and the ileocecal junction. The distance from the pyloric sphincter to the ileocecal junction was considered to reflect the whole length of the small intestine. The distance from the pylorus to the frontier of activated charcoal was measured as the migration distance. The gastrointestinal transit (GIT) rate was calculated using the following formula:

$$\text{GIT rate}\,(\%) = [\text{MAC}/\text{LSI}] \times 100$$

where MAC and LSI represent the migration distance of activated charcoal and the whole length of small intestine, respectively.

2.11 | Opioid tolerance

Opioid tolerance was evaluated by performing the formalin test after chronic morphine treatment. Briefly, animals were administered with vehicle, morphine (10 $mg{\cdot}kg^{-1}$, i.p.) or photocaged-morphine (10 $mg{\cdot}kg^{-1}$, i.p.) twice a day (within a 12 h interval) for 5 days. After each administration, the hind paw was directly irradiated for 15 min with a LED-based fibre-optic system (Doric Lenses Inc.) at 405 nm light or mock manipulated (dark). The 405 nm light regime consisted of pulses that lasted 500 ms each and were administered at 1 Hz frequency with 23 mW output power and 2000 mA intensity. After chronic treatment, the formalin animal model of pain was performed as described above.

2.12 | Morphine-induced conditioned place preference

The rewarding effects of morphine were evaluated using the conditioned place preference (CPP) paradigm, which was performed based on a modified protocol previously described (Maldonado et al., 1997). The apparatus consisted of two main square conditioning compartments (15 × 15 × 15 cm), with differences in texture ground surface (i.e. rough and smooth) and different black and white pattern walls (i.e. squared and zebra stripes patterns), separated by a triangular central area with sliding doors. The light intensity within the conditioning chambers was 30 lux. The CPP test consisted of three phases, as indicated in Figure 8a. During the preconditioning phase (day 1), drug-naive mice were placed in the middle of the central area with free access to both compartments for 18 min (Figure 8a). The time spent in each compartment was recorded. During the morning sessions of the conditioning phase (days 2 to 4), mice received vehicle (saline), morphine (10 $mg{\cdot}kg^{-1}$, i.p.) or photocaged-morphine(10 $mg{\cdot}kg^{-1}$, i.p.) followed by direct light-irradiation of the hind paw with a LED-based fibre-optic system (Doric Lenses Inc.) at 405 nm light (500 ms pulses, 1 Hz frequency, 2000 mA intensity and 23 mW output power) or mock manipulated (dark) for 15 min and then were immediately confined into the drug-paired conditioning compartment for 30 min. During the evening sessions of the conditioning phase (days 2 to 4) (Figure 8a), separated at least 6 h from the morning sessions, mice received vehicle followed by direct light-irradiation of the hind paw with a LED-based fibre-optic system at 405 nm light (500 ms pulses, 1 Hz frequency, 2000 mA intensity and 23 mW output power) or mock manipulated (dark) for 15 min and then were immediately confined into the vehicle-paired conditioning compartment for 30 min. Thus, a total of three pairings were carried out with vehicle, morphine or photocaged-morphine(drug-paired compartment) and three pairings with vehicle (vehicle-paired compartment). Treatments were counterbalanced as closely as possible between compartments. Finally, the post-conditioning phase (day 5, Figure 8a) was conducted exactly as the preconditioning phase, allowing mice to freely explore both compartments for 18 min. The time spent in each compartment was recorded. The CPP score was calculated as follows:- CPP score (s) = (Time spent in the drug-paired compartment during post-conditioning phase) − (Time spent in the drug-paired compartment during pre-conditioning phase).

2.13 | Naloxone-precipitated morphine withdrawal

The naloxone-precipitated withdrawal syndrome in morphine-dependent mice was evaluated based on a modified protocol previously described (Maldonado et al., 1997). Briefly, animals were administered with vehicle, morphine (10 $mg{\cdot}kg^{-1}$, i.p.) or photocaged-morphine(10 $mg{\cdot}kg^{-1}$, i.p.) twice a day (within a 12 h interval) for 5 days, except for the last day when only the morning dose was administered. Immediately after each drug administration, the hind paw was directly irradiated with a LED-based fibre-optic system (Doric Lenses Inc.) at 405 nm light or mock manipulated (dark) for 15 min. The 405 nm light regime consisted of pulses that lasted 500 ms each and were administered at 1 Hz frequency with 23 mW output power and 2000 mA intensity. Afterwards, withdrawal was precipitated by injecting naloxone (1 $mg{\cdot}kg^{-1}$, s.c.) 2 h after the last morphine administration. Animals were placed individually into observational test chambers to evaluate the behavioural signs of withdrawal 10 min before naloxone administration and for 30 min immediately after naloxone injection. The chambers consisted of transparent round glass containers (20 cm in diameter) above a dark surface. Wet dog shakes, jumping, paw tremor and sniffing were counted over 5-min periods. Teeth chattering, piloerection, ptosis, diarrhoea and tremor were scored 1 for appearance or 0 for nonappearance within each 5-min period. Locomotor activity over 5-min periods was rated 0 (normal activity), 1 (low activity) or 2 (inactivity). Body weight was determined the first day and the last day (before naloxone injection). Considering all the individual signs, a global withdrawal score was calculated for each animal, as previously reported (Maldonado et al., 1992), by giving each individual sign a relative weight: 0.5 for each episode of wet dog shake, jumping, paw tremor or sniffing; and 1 for the presence of teeth chattering, piloerection, ptosis, diarrhoea and tremor during each observation

period of 5 min. Locomotor activity score for each period was added to the global withdrawal score.

2.14 | Data and statistical analysis

The data and statistical analysis in this study comply with the recommendations of the British Journal of Pharmacology on experimental design and analysis in pharmacology (Curtis et al., 2018). Data are represented as mean ± standard error of mean (SEM) with statistical significance set at $P < 0.05$. The number of samples/animals (n) in each experimental condition is indicated in the corresponding figure legend. Statistical analysis was undertaken only for data sets where each group size was at least $n = 5$. Outliers were assessed by the Iterative Grubbs' test; no animals were excluded. Comparisons among experimental groups were performed by two- or three-way factor ANOVA followed by Tukey's multiple comparisons post hoc test using GraphPad Prism 9 (RRID: SCR_002798; San Diego, CA, USA), as indicated.

2.15 | Materials

The commercial suppliers for chemical were Acefe, Gavà, Spain; Panreac Química, Castellar del Vallès, Spain; and Fisher Scientific, Madrid, Spain. All the other suppliers are alreaded provided.

2.16 | Nomenclature of targets and ligands

Key protein targets and ligands in this article are hyperlinked to corresponding entries in the IUPHAR/BPS Guide to PHARMACOLOGY http://www.guidetopharmacology.org and are permanently archived in the Concise Guide to PHARMACOLOGY 2019/20 (Alexander et al., 2019).

3 | RESULTS

3.1 | Design and synthesis of photocaged morphine

To generate a morphine-based photosensitive compound (photocaged-morphine), we applied a caging strategy based on the chemical binding of morphine to a photoremovable coumarine (i.e. coumarinyl phototrigger, Figure 1). Thus, we synthesized photocaged-morphine by tethering one of the hydroxyl groups of morphine to a bromoderivative of the violet-light absorbing coumarin DEACM in a one-pot procedure.

Next, we evaluated the UV–visible absorption spectrum of the newly synthesized compound. As shown in Figure 2a, photocaged-morphine showed a maximum absorption peak at 394 nm, resembling that of the coumarin unit, thus in agreement with the lack of absorption in the visible region of morphine. Subsequently, we assessed the photocaged-morphine photochemical behaviour upon 405 nm light irradiation. Under these experimental conditions, spectral changes consistent with the photolysis of the coumarin benzylic bond and release of the appended morphine fragment were observed (Figure 2b) (Wong et al., 2017). This was further ascertained by MS analysis after photocaged-morphine photolysis (Figure S1). A quantum yield of $\Phi_{chem} = 0.004$ was determined for the uncaging process of photocaged-morphine, which is in reasonable agreement with the photochemical behaviour reported for other biologically-relevant hydroxyl groups caged with

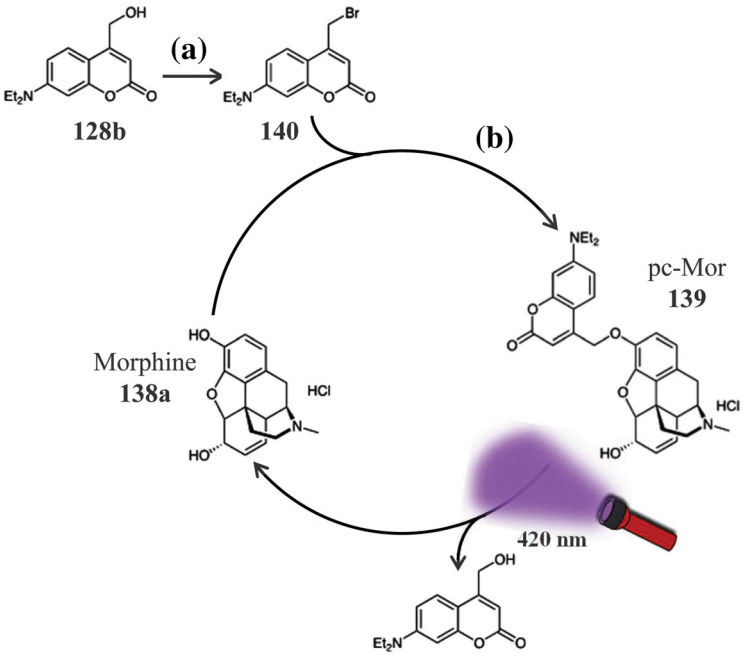

FIGURE 1 Design and synthesis of photocaged morphine. The synthesis of photocaged-morphine (pc-Mor) from morphine involves a one-pot procedure using morphine and 7-(diethylamino)-4-(hydroxymethyl)coumarin (DEACM, 128b). Conditions: (a) NEt_3, MsCl, LiBr, DCM, THF, r.t., 3 h, 44%. (b) K_2CO_3, DMF, r.t., 4 days, 47% (see Section 2)

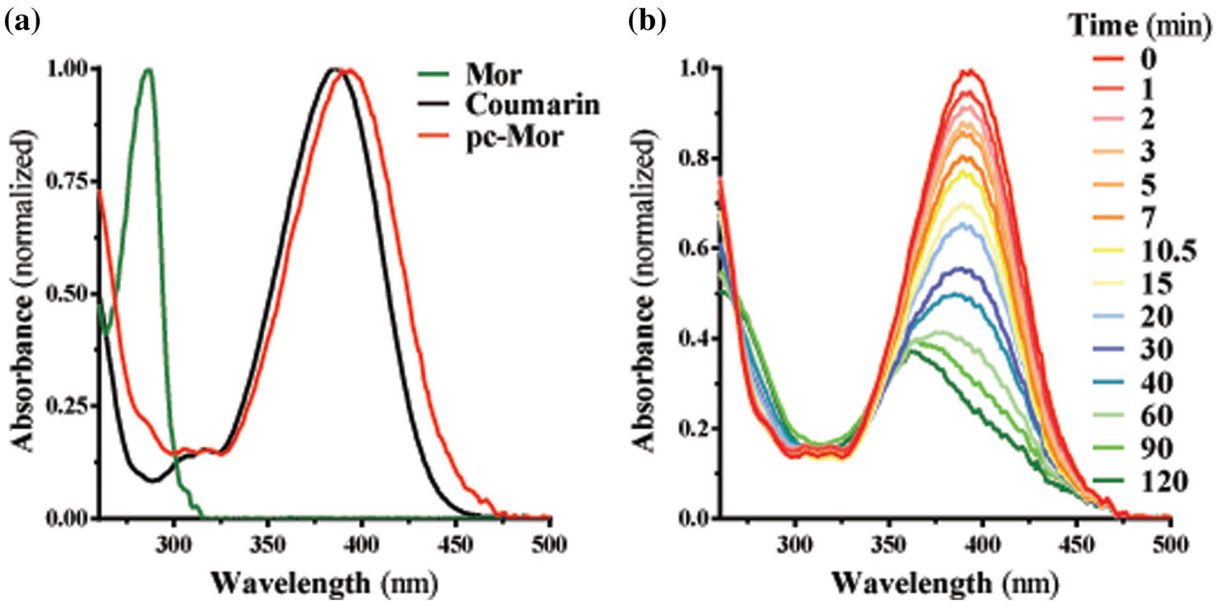

FIGURE 2 Photochemical properties of photocaged-morphine (pc-MOR). (a) Absorption spectra of pc-Mor and its separate morphine and 7-(diethylamino)-4-(hydroxymethyl)coumarin (DEACM; coumarin)) units in PBS:DMSO 99:1 ($c = 7.0$ μM). For comparison purposes, the maximum of the spectra is normalized to unity. (b) Variation of the absorption spectrum of pc-Mor in PBS:DMSO 99:1 ($c = 7.0$ μM) upon continuous excitation at 405 nm (0.56 W·cm^{-2}; irradiation time = 0, 1, 2, 3, 5, 7, 10.5, 15, 20, 30, 40, 60, 90 and 120 min)

7-diethylamino-4-hydroxymethylcoumarin through an ether linkage (Wong et al., 2017).

3.2 | Optical control of μ-opioid receptor in cultured cells and primary neurons

To assess photocaged-morphine-mediated photocontrol of μ receptors, we first evaluated intracellular calcium accumulation (Hauser et al., 1996) in stable MOR-expressing HEK cells. While morphine (100 nM) induced a robust intracellular calcium rise both in dark and under 405 nm illumination, photocaged-morphine (100 nM) only produced intracellular calcium accumulation upon irradiation with 405 nm light (Figure 3a). In line with this, morphine concentration-dependently increased intracellular calcium levels, both in dark and light conditions ($pEC_{50} = 8.21 \pm 0.18$ and $pEC_{50} = 8.01 \pm 0.21$, respectively) (Figure 3b). Conversely, photocaged-morphine only elicited a concentration-dependent increase in calcium accumulation upon irradiation with 405 nm light (Figure 3b), with a similar potency to that observed for morphine ($pEC_{50} = 7.90 \pm 0.25$). Next, we assessed light-dependent μ receptor-mediated GIRK activation. We co-transfected GIRK-1 and GIRK-2 subunits in stable μ receptor-expressing HEK cells and performed voltage-clamp experiments. Cells were selected for recording based on their plasma membrane expression of GIRK1-YFP (Figure 3c), voltage-clamped at −80 mV and the morphine and photocaged-morphine were applied while the inward current was monitored (Figure 3d). Under these experimental conditions, morphine evoked a concentration-dependent GIRK-mediated inwardly rectifying current ($pEC_{50} = 6.90 \pm 0.12$) (Figure 3e), as expected (Johnson et al., 2006). Again, photocaged-morphine was able to induce a concentration-dependent GIRK-mediated current only following irradiation with 405 nm light ($pEC_{50} = 6.53 \pm 0.11$) (Figure 3c), thus validating the caging approach to photocontrol the intrinsic activity of this μ receptor caged agonist.

Finally, we performed intracellular calcium accumulation experiments in cultured neurons from mouse dorsal root ganglion (DRG; Figure 4a), to assess the light-dependent activity of photocaged-morphine in a native system. Similar to that observed in stable μ receptor-expressing HEK cells, while morphine was able to induce a significant increase in calcium levels both in dark and under 405 nm illumination (Figure 4b,c), photocaged-morphine only elicited intracellular calcium accumulation upon irradiation with 405 nm light (Figure 4b,c). Analysis (Treatment × Illumination) revealed a significant main effect of treatment, illumination and the interaction between both factors was also highly significant between dark and 405 nm illumination conditions in photocaged-morphine treated DRGs (Figure 4c). Of note, we also aimed at recording electrophysiology responses to morphine and photocaged-morphinein cultured DRGs but were unable to register consistent electrophysiological responses (Figure S3). These results could be due to the fact that DRGs are known to form a rather heterogeneous population, with only small subsets expressing GIRK channel subunits and μ receptors, respectively, at the mRNA level (Usoskin et al., 2015). Nevertheless, calcium recordings, which allowed to assess μ receptor-dependent activity in the whole cell population, confirmed the ability of photocontrolling the intrinsic activity of photocaged-morphine both in heterologous and endogenous systems.

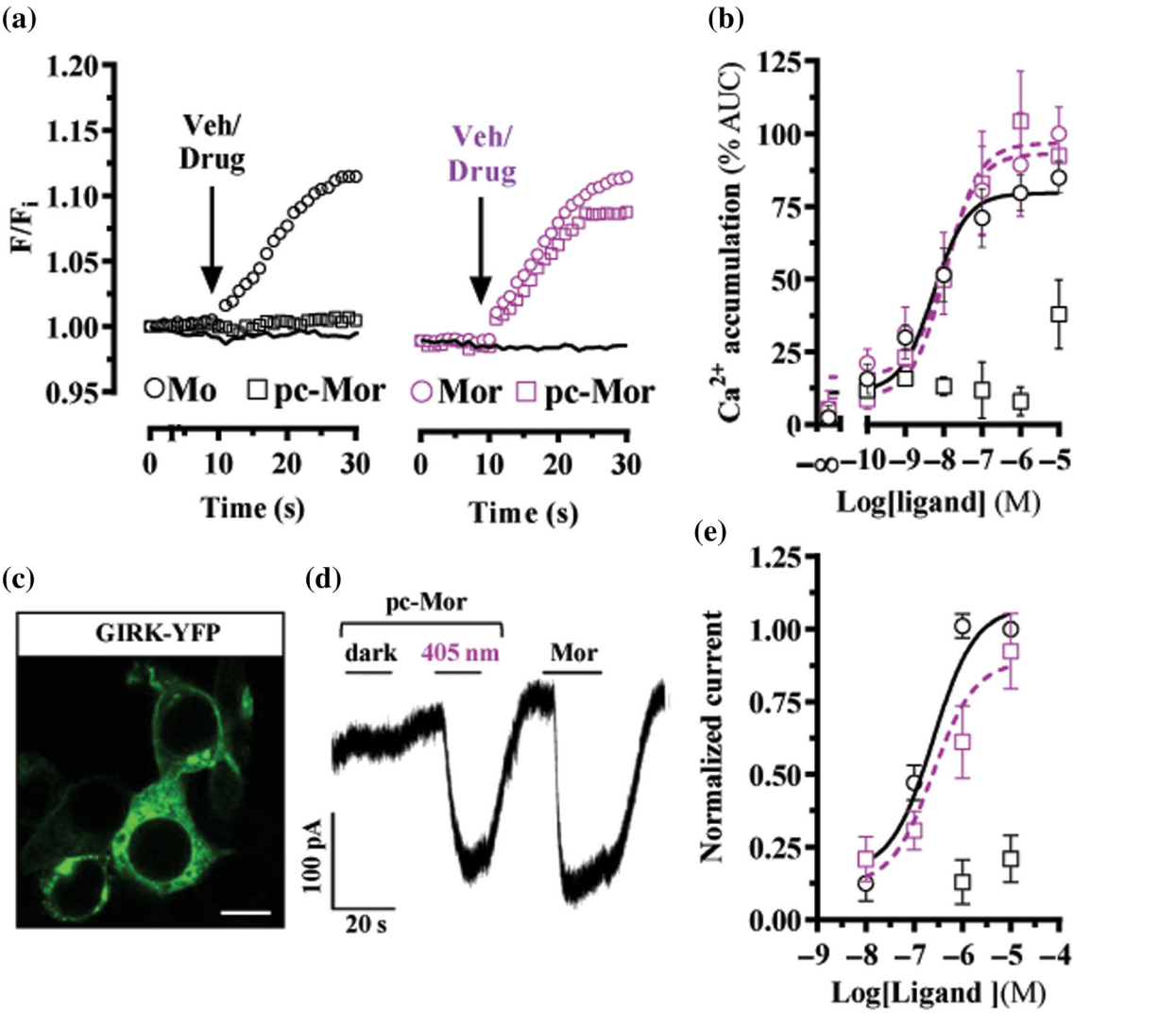

FIGURE 3 Optical modulation of μ receptor activity in living cells. (a) Determination of morphine (MOR)-mediated intracellular calcium mobilization in HEK-293T cells stably expressing MOR. Representative time course of intracellular calcium mobilization in cells incubated with vehicle (Veh), morphine (MOR, 100 nM) or photocaged-morphine (pc-MOR, 100 nM) while monitoring intracellular calcium accumulation in dark (left panel) or upon irradiation at 405 nm (right panel). (b) Concentration-response photo-modulation of MOR-mediated calcium accumulation. The AUC (AUC) of intracellular calcium accumulation in HEK-293T cells stably expressing MOR treated with morphine (circle) or pc-MOR (square) in dark (black) or irradiated at 405 nm (violet) was quantified. All the values are expressed as percentage of the corresponding ionomycin signal (mean ± SEM; $n = 5$). (c) Representative image of GIRK-YFP expression in HEK-293T cells stably expressing MOR and transiently transfected with GIRK1-YFP and GIRK2. Cells were analysed by fluorescence microscopy. Scale bar: 10 μm. (d) Representative GIRK current recording from HEK-293T cells stably expressing MOR and transiently transfected with GIRK1-YFP and GIRK2. Cells were voltage-clamped at −80 mV, superfused with high-potassium buffer, and exposed to 1 μM of morphine (MOR), pc-MOR or pc-MOR irradiated at 405 nm. (e) Concentration-response curves of evoked GIRK currents. Increasing concentrations of morphine (circle) or pc-MOR (square) in dark (black) or irradiated at 405 nm (violet) were superfused to cells and the increase in inward current was taken as a measure of MOR activation. Results were plotted as a fraction of the maximal response to 10 μM morphine in each cell (mean ± SEM; $n = 5$)

3.3 | Photocontrolling morphine-mediated antinociception

One of the main goals of developing a morphine-based photopharmacology strategy was to achieve pain management with high spatiotemporal resolution. We first assessed the ability of photocaged-morphine to elicit light-dependent antinociception in an animal model of pain. We took advantage of the formalin mouse model of pain, since it allows for the assessment of both peripheral and central receptors within the pain neuraxis (Mogil, 2009). We investigated light-dependent photocaged-morphine antinociceptive effects by irradiating peripheral (hind paw) and central (spinal cord) tissues (Figures 5 and 6, respectively). First, following the protocol indicated in Figure 5a, we administered vehicle, morphine or photocaged-morphine and assessed its antinociceptive effects in dark and light conditions upon peripheral (hind paw) 405 nm irradiation (Figure 5a,

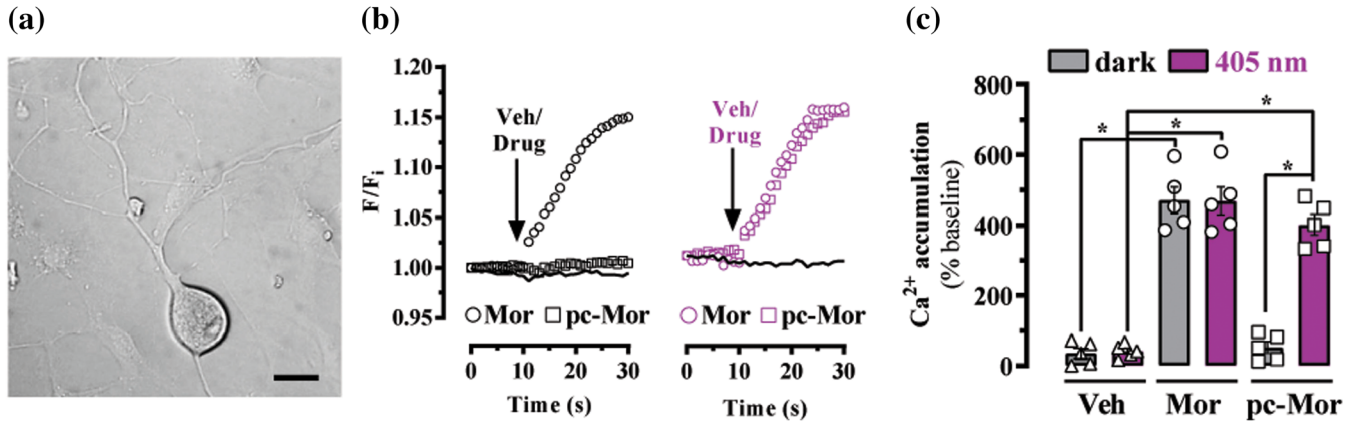

FIGURE 4 Optical modulation of endogenous μ receptor activity in primary DRG neurons. (a) Brightfield image of a primary mouse DRG neuron at 1 day in vitro. Scale bar: 10 μm. (b) Determination of morphine-mediated intracellular calcium accumulation in primary DRG neurons. Representative time course of intracellular calcium mobilization in neurons incubated with vehicle (Veh), morphine (MOR, 100 nM) or photocaged morphine (pc-MOR, 100 nM) while monitoring intracellular calcium accumulation in dark (left panel) or upon irradiation at 405 nm (right panel). (c) Quantification of photo-modulation of MOR-mediated calcium accumulation. The AUC (AUC) of intracellular calcium accumulation in DRG neurons treated with vehicle (Veh), morphine (MOR, 100 nM) or photocaged morphine (pc-MOR, 100 nM) in dark (black) or upon irradiation at 405 nm (violet) was quantified. All the values are expressed as percentage of the corresponding ionomycin signal (mean ± SEM; $n = 5$). *$P < 0.05$, two-way ANOVA with Tukey's post hoc test

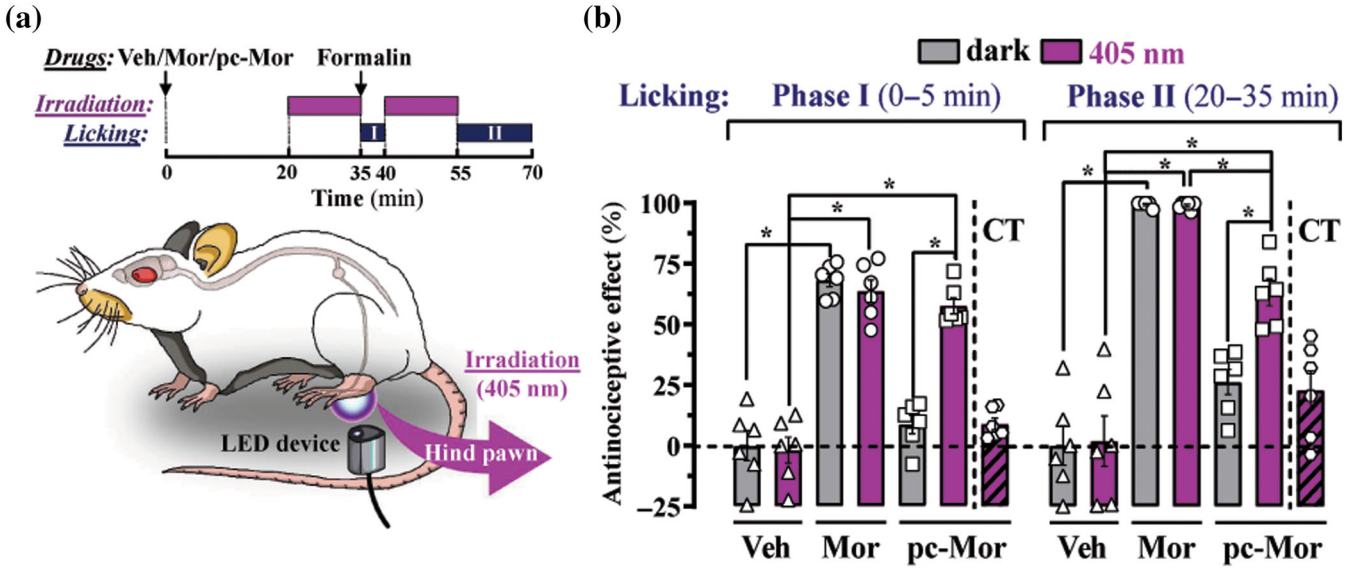

FIGURE 5 Optical control of peripheral μ receptors in the formalin animal model of pain. (a) Upper part: Scheme of the 405 nm irradiation regime (violet rectangles) and licking recordings (grey rectangles – Phase I and phase II) in the formalin animal model of pain. Thus, animals were intraperitoneally injected with vehicle (Veh, saline), morphine (Mor, 10 mg·kg^{-1}) or photocaged-morphine (pc-Mor, 10 mg·kg^{-1}) 20 min before irradiation at 405 nm or mock manipulated (dark) for 15 min. Lower part: Graphical scheme showing the LED-mediated irradiation of the hind paw. (b) Peripheral light-dependent pc-Mor-mediated antinociception in mice was assessed upon irradiation of the hind paw (see Section 2). Total hind paw licking was measured for 0–5 min (phase I) and 15–30 min (phase II) after intraplantar injection of 20 μl of formalin solution (2.5% paraformaldehyde). As a control of peripheral pc-Mor uncaging, the contralateral hind paw (CT) was also irradiated. The antinociceptive effect was calculated as the percentage of the maximum possible effect (see Section 2) and expressed as mean ± SEM ($n = 6$). *$P < 0.05$ two-way ANOVA with Tukey's post hoc test

lower panel). As previously reported (López-Cano et al., 2019), formalin injection induced an innate defensive licking/biting behaviour, which was not modified upon vehicle injection, neither in dark nor in light conditions (Figure 5b). Analysis of treatment × illumination confirmed a significant main effect of treatment on illumination and the interaction between both factors in phase I and II. Thus, systemic morphine administration (10 mg·kg^{-1}, i.p.) produced significant antinociceptive effects, both in phases I and II of the formalin test, and

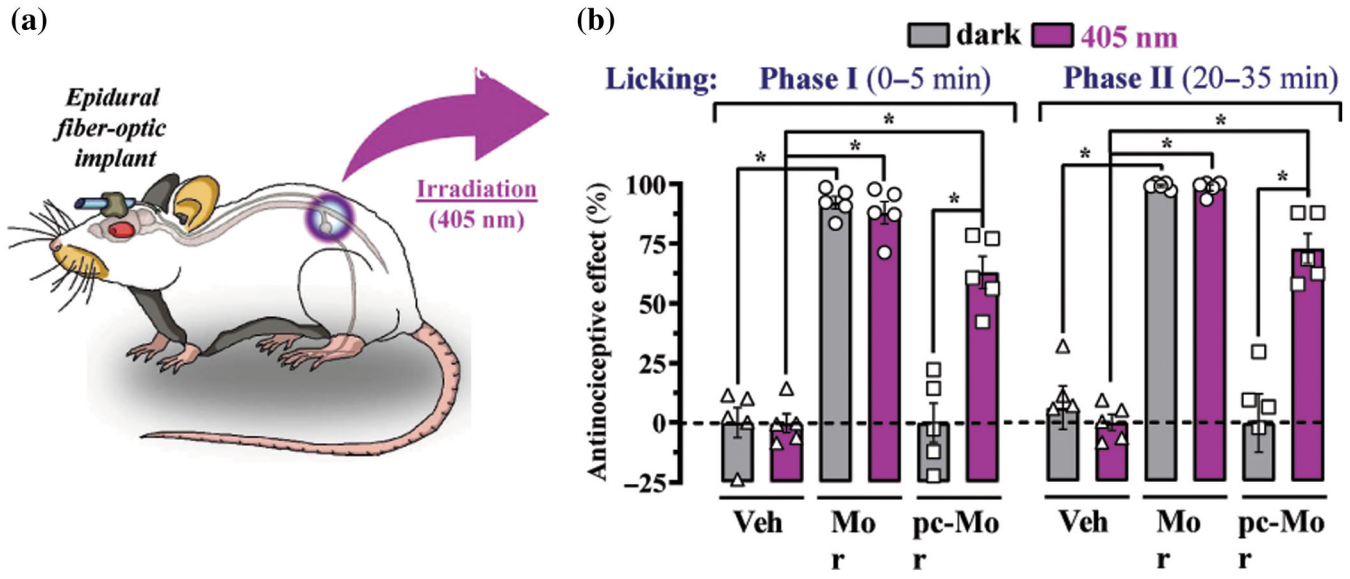

FIGURE 6 Optical control of central μ receptors MORs in the formalin animal model of pain. (a) Graphical scheme showing the irradiation of the lumbar region using a LED-based epidural fibre-optic implant. (b) Central light-dependent pc-Mor-mediated antinociception in mice was assessed upon irradiation of the spinal cord (see Section 2). Total hind paw licking was measured for 0–5 min (phase I) and 15–30 min (phase II) after intraplantar injection of 20 μl of formalin solution (2.5% paraformaldehyde). The antinociceptive effect was calculated as the percentage of the maximum possible effect (see Section 2) and expressed as mean ± SEM ($n = 6$). *$P < 0.05$, two-way ANOVA with Tukey's post hoc test

regardless of light irradiation (Figure 5b). Of note, while morphine was able to completely abolish formalin pro-nociceptive effects at phase II, it only partially reduced nociception at phase I (Figure 5b). These results indicate that morphine was more effective at relieving central sensitization than acute peripheral pain. On the other hand, when administering photocaged-morphine(10 mg·kg^{-1}, i.p.) in dark conditions we did not observe a significant antinociceptive effect, compared with vehicle treated animals (Figure 5b). Importantly, while photocaged-morphine was unable to suppress nociceptive responses in dark conditions, it did elicit significant antinociceptive effects after direct hind paw irradiation, both in phase I and II (Figure 5b). This result confirmed that, after systemic administration, photocaged-morphine was peripherally photo-uncaged and induced antinociceptive effects. Subsequent analysis revealed that the light-dependent photocaged-morphine antinociceptive effects in phase II were significantly lower than that observed for morphine (63.3 ± 13.6% vs. 99.1 ± 1.5%), a difference likely explained by either the limited local (non-central) effects of photocaged-morphine upon hind-paw irradiation or the inability to photo-release all the drug systemically administered. Importantly, photocaged-morphine did not display antinociceptive effects when the contralateral hind paw (CT, non-injected with formalin) was irradiated (Figure 5b).

Given the higher efficacy of morphine relieving central sensitization and aiming to develop a potential translational approach to photocontrol opioid-mediated effects, we next evaluated the antinociceptive effects of photocaged-morphine after epidural irradiation (Figure 6a). Although the implantation of a flexible fibre-optic at the lumbar epidural anatomical area did not affect the nociceptive responses to formalin injection (Figure 6b), all animals underwent surgery and were submitted to the irradiation protocol either they were treated with photocaged-morphine or not. There was a significant main effect of treatment in both phase I and II and with illumination also with the interaction between both factors. Again, morphine (10 mg·kg^{-1}, i.p.) was able to exert antinociceptive effects both at phases I and II, regardless of light irradiation (Figure 6b). Interestingly, photocaged-morphine (10 mg·kg^{-1}, i.p.) was only able to suppress formalin-induced nocifensive behaviour when light was delivered to the epidural anatomical space (Figure 6b). Thus, while photocaged-morphine did not display antinociceptive effects in dark conditions, it significantly inhibited nociception both in phase I (62.1 ± 15.1%) and in phase II (72.6 ± 14.2%) upon direct spinal cord illumination and confirmed with a Tukey's post hoc test. Epidural uncaged photocaged-morphine had comparable efficacy to systemic morphine in phase II (72.6 ± 14.2% vs. 98.2 ± 2.8%). It seems likely that central μ receptors contribute to a higher extent to block central sensitization (i.e. phase II in the formalin animal model of pain). Overall, these results demonstrated that photocaged-morphine was effective in mediating antinociception both upon peripheral and central irradiation. In other words, our data support the notion that localized light irradiation targeting peripheral and spinal μ receptors might represent a valuable strategy for the treatment of pain-related diseases.

3.4 | Reduction of tolerance and opioid-related side effects upon photocaged-morphine treatment

Opioid-based analgesic therapies may lead to tolerance to the analgesic effects and a series of side effects (i.e. constipation, dependence

and addiction) (Grim et al., 2020). Thus, one of the main aims of a morphine-based photopharmacology strategy may consist of attempting to minimize these undesired side effects. First, we assessed the putative tolerance to analgesic effects of chronic photocaged-morphine treatment, as compared with that developed by morphine. Mice were chronically administered with vehicle, morphine or photocaged-morphine before the formalin-induced behaviour was assessed. There was a significant main effect of treatment in Phase I and II for illumination, drug regime, the interaction between treatment and illumination and the interaction between treatment and drug regime, but not between drug regime and illumination or treatment, illumination and drug regime in both phases of the formalin test. As expected, chronic morphine administration led to the significant development of tolerance to its antinociceptive effects, after its chronic administration at phase I and II both in light and dark conditions (Figure 7). Chronic photocaged-morphine administration did not lead to tolerance as no significant differences in the antinociceptive effects between acute and chronic of photocaged-morphine treatment at phase I and II both in light and dark conditions were found (Figure 7).

Next, we evaluated the possibility that photocaged-morphine induced constipation, one of the most unpleasant side effects of chronic opioid use and withdrawal cited by patients (Farmer et al., 2018). We examined gastrointestinal transit in mice receiving systemic administration of vehicle, morphine, or photocaged-morphine. As shown in Figure 8a, morphine produced a marked light independent inhibition of gastrointestinal transit, as expected (Manara et al., 1986). There was a significant effect of treatment but no significant effect of illumination or the interaction between both factors. Importantly, although there was significant inhibition of gastrointestinal transit in morphine administered animals both in dark and upon hind paw irradiation, photocaged-morphine did not produce a change in gastrointestinal transit, neither in dark nor in light conditions (Figure 8a). These results may support the use of photocaged-morphine as a potentially effective way to achieve antinociception while avoided the undesirable systemic off-target effects of chronic opioid use.

It seems clear that tolerance and constipation are some of the many factors that contribute to making long term opioid-based therapies for pain both difficult and uncomfortable. However, based on epidemiological data from the last few years, the main issues concerning opioid-based treatments relate to the misuse and abuse of these kinds of drugs (Koob, 2020). We aimed to determine whether systemic administration and photoactivation of photocaged-morphine could circumvent the development of morphine-mediated dependence. First, we evaluated the rewarding effects of photocaged-morphine by using a conditioned place preference (CPP) paradigm (Figure 8b), a standard behavioural model used to study the rewarding and aversive effects of drugs, including opiates, in rodents (Maldonado et al., 1997). A significant effect of drug treatment was identified, whereas there was no significant effect of illumination or the interaction between both factors was observed. However, subsequent Tukey's post hoc test revealed an expected significant increase in the time spent in the drug-associated compartment upon repeated

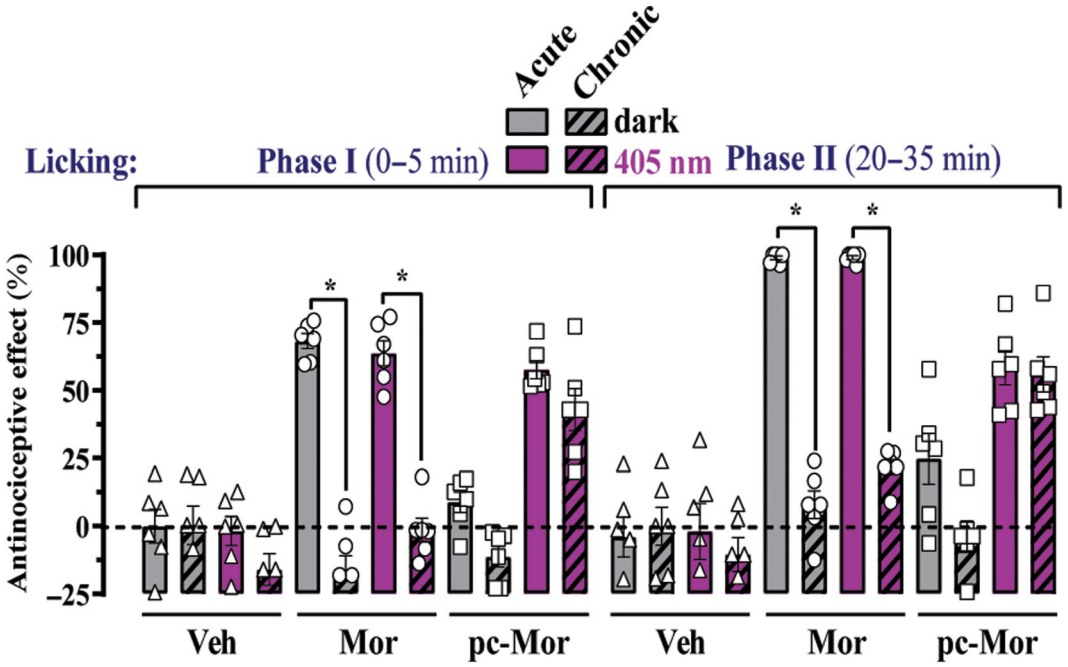

FIGURE 7 Reduced opioid-induced tolerance upon morphine photocontrol. Animals were chronically (twice a day during 5 days) administered with vehicle (Veh, saline, i.p.), morphine (Mor, 10 mg·kg^{-1}, i.p.) or photocaged morphine (pc-Mor, 10 mg·kg^{-1}, i.p.) 20 min before hind paw light irradiation (see Section 2 and Figure 5a). Finally, on the last day of treatment, antinociception was determined and the results compared with that obtained upon acute treatment. The antinociceptive effect was calculated as the percentage of the maximum possible effect (see Section 2) and expressed as mean ± SEM ($n = 6$). *$P < 0.05$, three-way ANOVA with Tukey's post hoc test

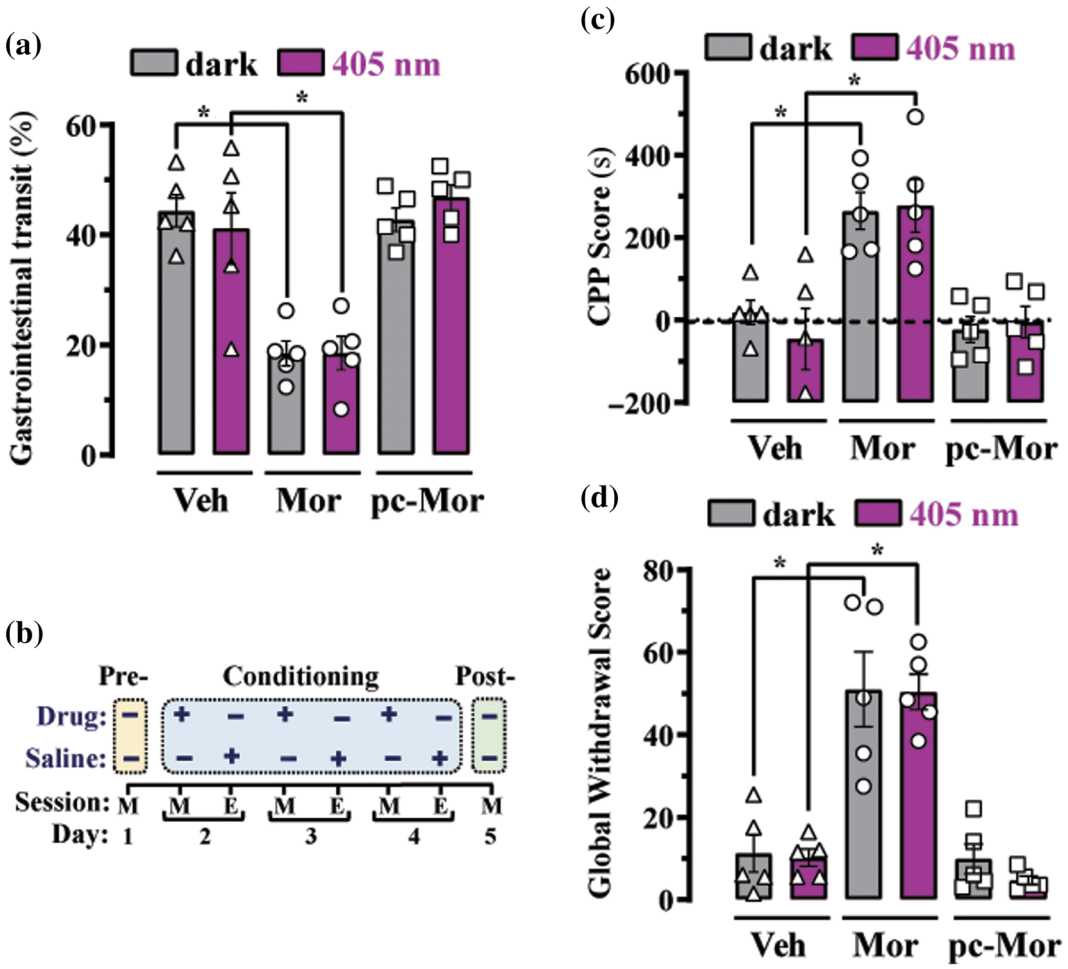

FIGURE 8 Pc-morphine induce minimal adverse side effects. (a) Gastrointestinal transit (GIT) assessment. Effect of vehicle (Veh), morphine (Mor, 10 mg·kg^{-1}, i.p.) and photocaged-morphine (pc-Mor, 10 mg·kg^{-1}, i.p.) in GIT. Results are represented as percentage of activated charcoal transit according to total length of intestine (see material and Methods) and expressed as mean ± SEM ($n = 5$). *$P < 0.05$, two-way ANOVA with Tukey's post hoc test. (b) Experimental schedule to determine morphine induced CPP in mice. The three experimental behavioural phases (i.e. preconditioning, conditioning and postconditioning) with the corresponding pairing treatment (i.e. drug-saline) per session (M, morning and E, evening) and day is indicated. (c) Morphine-induced CPP. Animals were treated with vehicle (Veh, saline), morphine (Mor, 10 mg·kg^{-1}) or photocaged-morphine (pc-Mor, 10 mg·kg^{-1}) following the pairing schedule shown in panel (b), as described in materials and Methods section. The CPP score was calculated and expressed as mean ± SEM ($n = 5$). *$P < 0.05$,two-way ANOVA with Tukey's post hoc test. (d) Naloxone-precipitated morphine withdrawal. Animals were chronically treated with vehicle (Veh, saline, i.p.), morphine (Mor, 10 mg·kg^{-1}, i.p.) or photocaged-morphine (pc-Mor, 10 mg·kg^{-1}, i.p.) 20 min before hind paw irradiation (see Section 2 and Figure 5a). After last drug administration, withdrawal was precipitated by administering naloxone (1 mg·kg^{-1}, s.c.). the global withdrawal score was calculated considering all the physical signs (i.e. wet dog shakes, jumping, paw tremor, sniffing, teeth chattering, piloerection, ptosis, diarrhoea, tremor and/or decreased locomotor activity) and expressed as mean ± SEM ($n = 5$). *$P < 0.05$, two-way ANOVA with Tukey's post hoc test

morphine administration, independently of irradiation (Figure 8c). Conversely, photocaged-morphine treatment did not induce drug-mediated place preference, neither in dark nor in light conditions (Figure 8c). Overall, these results indicated that photocaged-morphine was devoid of rewarding properties, indicating that locally released morphine would not mediate central effects responsible for opioid dependence.

Finally, we evaluated the development of a withdrawal syndrome, which is a severe opioid-related side-effect. Mice receiving daily drug (i.e. vehicle, morphine or photocaged-morphine) injections were subsequently administered with naloxone (1 mg·kg^{-1}) to precipitate withdrawal. Again, a significant effect of drug treatment was identified, whereas there was no significant effect of illumination or the interaction between both factors was observed. No signs of withdrawal were observed in any group of mice during behavioural observation before the administration of naloxone. Naloxone administration did not exert any relevant effect on vehicle-injected mice. Importantly, while in chronic morphine-treated mice naloxone injection precipitated a significant withdrawal syndrome manifested by the presence of several somatic signs (i.e. wet dog shakes, paw tremor, jumps, ptosis, decreased locomotor activity and diarrhoea), in mice chronically treated with photocaged-morphine no withdrawal

syndrome was observed (Figure 8d). Overall, our data provide promising indications concerning a potential novel opioid-based treatment, in which analgesic effects could be achieved with reduced adverse effects and no analgesic tolerance.

4 | DISCUSSION

The use of opioids for pain relief involves major concerns, the possible appearance of tolerance to their analgesic effects and adverse side effects, such as constipation and dependence. In recent years, due to high prescription rates, opioid-related side effects have become a major health problem (Volkow & Thomas McLellan, 2016). Here, we provide compelling evidence for a novel pharmacological approach, based on the use of light to control drug activity and reach effective pain treatment without these opioid-related undesired effects. To our knowledge, photocaged-morphine is the first caged morphine derivative that has shown light-dependent analgesic effects, while it did not produce constipation, tolerance or a naloxone-induced withdrawal, and had no rewarding effects when activated peripherally by light. The protocol of light administration included the use of external and internal LED-based irradiation, allowing for local photocaged-morphine activation in the hind paw and the spinal cord, respectively. Accordingly, this new photopharmacological approach may provide an optimal benefit/risk ratio for opioid-based therapies, which can propel its rapid translation into clinical settings.

Photopharmacology, or the ability of light to control the biological activity of drugs by changing their pharmacokinetic or pharmacodynamic profile (Hüll et al., 2018), has the advantage of providing high spatial and temporal resolution to drug action and reaction. However, the usual need for implantation of fibre-optics in the brain may limit its use in clinical settings. Our work is a first-line proof-of-concept study that may prompt the transition from preclinical to clinical light-based devices. However, it is important to note that further preclinical work is still needed before implementing this photopharmacological approach into a more clinical context. Some of the potential limitations are (i) we used a single photocaged-morphine dose (10 $mg \cdot kg^{-1}$), based on previous experience (Font et al., 2017). In addition, it would be valuable to assess morphine levels after photocaged-morphine photo-uncaging, both at plasma and target tissues, to establish the exact dosage for each route of administration; (ii) we only used a single paradigm of inflammatory pain (i.e. formalin mouse model). It would be needed to assess the effectiveness of photocaged-morphine in other animal models of pain and (iii) we determined a number of undesired effects (i.e. constipation, dependence) but it would be important to assess one of the major concerns when using opioids, which is respiratory depression (McNicol et al., 2003). In addition, it would be relevant to assess how the use of photo-caged drugs may influence on emotional aspects of pain, which indeed have limited the transition of a number of pain-related assays from animals to humans. On the other hand, the present photopharmacology approach is an excellent tool to dissect the mechanism of action of opioids in the periphery and the CNS, thus this technology may allow to address important questions in the field.

Several issues should be considered when using light as a precision tool in pharmacology. The first, and more obvious issue, consists of the way to deliver light into the target tissue. As commented above, in some previous works, fibre-optics were implanted into the brain (Font et al., 2017). Here, we took advantage of less-invasive procedures to administer light. Thus, we used external (hind paw) and internal (epidural) fibre-optics, previously implemented in pain control (Bonin et al., 2016; Font et al., 2017). Another important issue when implementing photopharmacology is the wavelength used to achieve drug photoactivation. Thus, most photoactivable compounds require UV light irradiation that may readily photodamage biological tissues (Patton et al., 1999) and display poor tissue penetration (Frangioni, 2003). Interestingly, a series of coumarin photocleavable protecting groups, as the one used in this study, which enable the conditional release of biologically active ligands at 405 nm, have been developed (Klán et al., 2013) and implemented for *in vitro* and *in vivo* use with non-toxic effects (Font et al., 2017; Taura et al., 2018). Furthermore, novel drugs are currently being synthesized aiming to use red-shifted wavelengths, which display higher tissue penetration (Li et al., 2014; Wegener et al., 2017).

The use of light might allow for the circumvention of the important opioid-related drawbacks, mostly related to their abuse and/or misuse. Indeed, prescribed opioid analgesics can be abused by taking the medication at or above the recommended dosage via the intended route of administration (Katz et al., 2011). In addition, opioid drugs can be manipulated to be administered through alternative routes (i.e. inhalation), which have been correlated with the increased efficacy of these drugs and an increase likelihood to develop dependency (Samaha & Robinson, 2005). Extended-release opioid formulations designed for around-the-clock management of severe pain are very attractive to abusers, since they contain a great amount of drug as compared with that found in immediate-release formulations (Kirsh et al., 2012). To minimize the risk of manipulating prescribed drugs, novel opioid formulations have been designed (Alexander et al., 2014; Lourenço et al., 2013). These formulations, termed as abuse-deterrent formulations, include physical and chemical barriers to prevent manipulation of the formulation and extraction of the active ingredient, combination with an antagonist, aversion technologies, use of new molecular entities or prodrugs, and novel delivery systems (Department of Health and Human Services Administration, 2015). The use of light in opioid-based therapies may not only represent a novel but also a superior abuse-deterrent formulation.

In conclusion, our results support the notion that light-based opioid drugs allow controlling analgesia in a time- and space-dependent manner. In addition, the use of photo-caged compounds may minimize the severe side effects associated with currently available opioid drugs.

ACKNOWLEDGMENTS

This work was supported by FEDER/Ministerio de Ciencia, Innovación y Universidades-Agencia Estatal de Investigación (SAF2017-87349-R,

SAF2017-87199-R and CTQ2017-89222-R), ISCIII (PIE14/00034), and the Catalan government (2017 SGR 1604 and 2017 SGR 465). We thank Centres de Recerca de Catalunya (CERCA) Programme/Generalitat de Catalunya for IDIBELL institutional support. We thank Esther Castaño and Benjamín Torrejón from the Scientific and Technical Services (SCT) group at the Bellvitge Campus of the University of Barcelona for their technical assistance. We thank Lourdes Muñoz, Carme Serra and Juanlo Catena (SimChem, IQAC-CSIC, Barcelona) for support in the synthesis of compounds. Xavier Gasull and Aida Castellanos (Facultat de Medicina, Universitat de Barcelona) are acknowledged by their help with the obtention of DRG neurons from mouse. Also, we thank María Pilar Pérez Villamor (Laboratorios Dr. Esteve, Barcelona) for the kind gift of the HEK293 cell line permanently expressing μ receptors.

AUTHOR CONTRIBUTIONS

M.L.-C., V.F.-D., E.A. and F.C. designed research; J.F. and A.L. conducted the chemical synthesis and analysed chemical data; G.C. and J.H. performed the photochemical studies; K.S. conducted the electrophysiology experiments; Y.D.-K. designed epidural fibre-optic experiments. M.L.-C., V.F.-D., E.A. and F.C. wrote the paper. All listed authors contributed to data collection, analysed data and/or revised the paper. V.F.-D., E.A. and F.C. supervised the research.

CONFLICT OF INTEREST

The authors declare no competing interest.

DECLARATION OF TRANSPARENCY AND SCIENTIFIC RIGOUR

This Declaration acknowledges that this paper adheres to the principles for transparent reporting and scientific rigour of preclinical research as stated in the *BJP* guidelines for Design and Analysis and Animal Experimentation, and as recommended by funding agencies, publishers and other organisations engaged with supporting research.

DATA AVAILABILITY STATEMENT

The data that support the findings of this study are available from the corresponding author upon reasonable request.

ORCID

Jesús Giraldo https://orcid.org/0000-0001-7082-4695
Yves De Koninck https://orcid.org/0000-0002-5779-9330
Francisco Ciruela https://orcid.org/0000-0003-0832-3739

REFERENCES

Alexander, L., Mannion, R. O., Weingarten, B., Fanelli, R. J., & Stiles, G. L. (2014). Development and impact of prescription opioid abuse deterrent formulation technologies. *Drug and Alcohol Dependence*, *138*, 1–6. https://doi.org/10.1016/j.drugalcdep.2014.02.006

Alexander, S. P. H., Christopoulos, A., Davenport, A. P., Kelly, E., Mathie, A., Peters, J. A., Veale, E. L., Armstrong, J. F., Faccenda, E., Harding, S. D., & Pawson, A. J. (2019). The concise guide to pharmacology 2019/20: G protein-coupled receptors. *British Journal of Pharmacology*, *176*, S21–S141.

Blyth, F. M., March, L. M., Brnabic, A. J. M., & Cousins, M. J. (2004). Chronic pain and frequent use of health care. *Pain*, *111*, 51–58. https://doi.org/10.1016/j.pain.2004.05.020

Bonin, R. P., Wang, F., Desrochers-Couture, M., Ga Secka, A., Boulanger, M. E., Côté, D. C., & De Koninck, Y. (2016). Epidural optogenetics for controlled analgesia. Mol. *Pain*, *12*, 1–11.

Cheung, C. W., Qiu, Q., Choi, S. W., Moore, B., Goucke, R., & Irwin, M. (2014). Chronic opioid therapy for chronic non-cancer pain: A review and comparison of treatment guidelines. *Pain Physician*, *17*, 401–414.

Clark, J. D., Gebhart, G. F., Gonder, J. C., Keeling, M. E., & Kohn, D. F. (1997). Special report: The 1996 guide for the care and use of laboratory animals. *ILAR Journal*, *38*, 41–48. https://doi.org/10.1093/ilar.38.1.41

Cousins, M. J., & Lynch, M. E. (2011). The declaration Montreal: Access to pain management is a fundamental human right. *Pain*, *152*, 2673–2674. https://doi.org/10.1016/j.pain.2011.09.012

Curtis, M. J., Alexander, S., Cirino, G., Docherty, J. R., George, C. H., Giembycz, M. A., Gilchrist, A., Hoyer, D., Insel, P. A., Izzo, A. A., Ji, Y., MacEwan, D. J., Sobey, C. G., Stanford, S. C., Teixeira, M. M., Wonnacott, S., & Ahluwalia, A (2018). Experimental design and analysis and their reporting: Updated and simplified guidance for authors and peer reviewers. *British Journal of Pharmacology*, *175*(7), 987–993. https://doi.org/10.1111/bph.14153

Department of Health and Human Services Administration, U.S.A. (2015). *Abuse-deterrent opioids: Evaluation and labeling*. Guidance for Industry.

Farmer, A. D., Holt, C. B., Downes, T. J., Ruggeri, E., Del Vecchio, S., & De Giorgio, R. (2018). Pathophysiology, diagnosis, and management of opioid-induced constipation. *The Lancet Gastroenterology & Hepatology*, *3*, 203–212. https://doi.org/10.1016/S2468-1253(18)30008-6

Font, J., López-Cano, M., Notartomaso, S., Scarselli, P., Di Pietro, P., Bresolí-Obach, R., Battaglia, G., Malhaire, F., Rovira, X., Catena, J., & Giraldo, J. (2017). Optical control of pain in vivo with a photoactive mGlu5 receptor negative allosteric modulator. *eLife*, *6*, e23545. https://doi.org/10.7554/eLife.23545

Frangioni, J. V. (2003). In vivo near-infrared fluorescence imaging. *Current Opinion in Chemical Biology*, *7*, 626–634. https://doi.org/10.1016/j.cbpa.2003.08.007

Grim, T. W., Acevedo-Canabal, A., & Bohn, L. M. (2020). Toward directing opioid receptor signaling to refine opioid therapeutics. *Biological Psychiatry*, *87*, 15–21. https://doi.org/10.1016/j.biopsych.2019.10.020

Hauser, K. F., Stiene-Martin, A., Mattson, M. P., Elde, R. P., Ryan, S. E., & Godleske, C. C. (1996). μ-Opioid receptor-induced Ca^{2+} mobilization and astroglial development: Morphine inhibits DNA synthesis and stimulates cellular hypertrophy through a Ca^{2+}-dependent mechanism. *Brain Research*, *720*, 191–203. https://doi.org/10.1016/0006-8993(96)00103-5

Higashiguchi, K., Matsuda, K., Asano, Y., Murakami, A., Nakamura, S., & Irie, M. (2005). Photochromism of dithienylethenes containing fluorinated thiophene rings. *European Journal of Organic Chemistry*, *2005*, 91–97.

Hüll, K., Morstein, J., & Trauner, D. (2018). In vivo photopharmacology. *Chemical Reviews*, *118*, 10710–10747. https://doi.org/10.1021/acs.chemrev.8b00037

Johnson, E. A., Oldfield, S., Braksator, E., Gonzalez-Cuello, A., Couch, D., Hall, K. J., Mundell, S. J., Bailey, C. P., Kelly, E., & Henderson, G. (2006). Agonist-selective mechanisms of μ-opioid receptor desensitization in human embryonic kidney 293 cells. *Molecular Pharmacology*, *70*, 676–685. https://doi.org/10.1124/mol.106.022376

Katz, N., Dart, R. C., Bailey, E., Trudeau, J., Osgood, E., & Paillard, F. (2011). Tampering with prescription opioids: Nature and extent of the problem, health consequences, and solutions. *The American Journal of Drug*

and Alcohol Abuse, *37*, 205–217. https://doi.org/10.3109/00952990.2011.569623

Kirsh, K., Peppin, J., & Coleman, J. (2012). Characterization of prescription opioid abuse in the United States: Focus on route of administration. *Journal of Pain & Palliative Care Pharmacotherapy*, *26*, 348–361. https://doi.org/10.3109/15360288.2012.734905

Klán, P., Šolomek, T., Bochet, C. G., Blanc, A., Givens, R., Rubina, M., Popik, V., Kostikov, A., & Wirz, J. (2013). Photoremovable protecting groups in chemistry and biology: Reaction mechanisms and efficacy. *Chemical Reviews*, *113*, 119–191. https://doi.org/10.1021/cr300177k

Kolodny, A., Courtwright, D. T., Hwang, C. S., Kreiner, P., Eadie, J. L., Clark, T. W., & Alexander, G. C. (2015). The prescription opioid and heroin crisis: A public health approach to an epidemic of addiction. *Annu. Rev Public Health*, *36*, 559–574. https://doi.org/10.1146/annurev-publhealth-031914-122957

Koob, G. F. (2020). Neurobiology of opioid addiction: Opponent process, hyperkatifeia, and negative reinforcement. *Biological Psychiatry*, *87*, 44–53. https://doi.org/10.1016/j.biopsych.2019.05.023

Law, P. Y., & Loh, H. H. (2013). Opioid receptors. In *Encyclopedia of biological chemistry* (Second ed., pp. 354–358). London, UK: Academic Press.

Lees, A. J. (1996). A photochemical procedure for determining reaction quantum efficiencies in systems with multicomponent inner filter absorbances. *Analytical Chemistry*, *68*, 226–229. https://doi.org/10.1021/ac9507653

Lerch, M. M., Hansen, M. J., van Dam, G. M., Szymanski, W., & Feringa, B. L. (2016). Emerging targets in photopharmacology. *Angewandte Chemie*, *55*, 10978–10999.

Li, W., Wang, J., Ren, J., & Qu, X. (2014). Near-infrared upconversion controls photocaged cell adhesion. *Journal of the American Chemical Society*, *136*, 2248–2251. https://doi.org/10.1021/ja412364m

Lilley, E., Stanford, S. C., Kendall, D. E., Alexander, S. P. H., Cirino, G., Docherty, J. R., George, C. H., Insel, P. A., Izzo, A. A., Ji, Y., Panettieri, R. A., Sobey, C. G., Stefanska, B., Stephens, G., Teixeira, M., & Ahluwalia, A. (2020). ARRIVE 2.0 and the *British Journal of Pharmacology*: Updated guidance for 2020. *British Journal of Pharmacology*, *177*, 3611–3616. https://doi.org/10.1111/bph.15178

Longo, P. A., Kavran, J. M., Kim, M.-S., & Leahy, D. J. (2013). Transient mammalian cell transfection with polyethylenimine (PEI). *Methods in Enzymology*, *529*, 227–240. https://doi.org/10.1016/B978-0-12-418687-3.00018-5

López-Cano, M., Font, J., Llebaria, A., Fernández-Dueñas, V., & Ciruela, F. (2019). Optical modulation of metabotropic glutamate receptor type 5 in vivo using a photoactive drug. *Methods in Molecular Biology*, *1947*, 351–359. https://doi.org/10.1007/978-1-4939-9121-1_20

Lourenço, L. M., Matthews, M., & Jamison, R. N. (2013). Abuse-deterrent and tamper-resistant opioids: How valuable are novel formulations in thwarting non-medical use? *Expert Opinion on Drug Delivery*, *10*, 229–240. https://doi.org/10.1517/17425247.2013.751095

Maldonado, R., Negus, S., & Koob, G. F. (1992). Precipitation of morphine withdrawal syndrome in rats by administration of mu-, delta- and kappa-selective opioid antagonists. *Neuropharmacology*, *31*, 1231–1241. https://doi.org/10.1016/0028-3908(92)90051-P

Maldonado, R., Saiardi, A., Valverde, O., Samad, T. A., Roques, B. P., & Borrelli, E. (1997). Absence of opiate rewarding effects in mice lacking dopamine D2 receptors. *Nature*, *388*, 586–589. https://doi.org/10.1038/41567

Manara, L., Bianchi, G., Ferretti, P., & Tavani, A. (1986). Inhibition of gastrointestinal transit by morphine in rats results primarily from direct drug action on gut opioid sites. *The Journal of Pharmacology and Experimental Therapeutics*, *237*, 945–949.

McDonald, J., & Lambert, D. G. (2016). Opioid mechanisms and opioid drugs. *Anaesthesia & Intensive Care Medicine*, *17*, 464–468. https://doi.org/10.1016/j.mpaic.2016.06.012

McNicol, E., Horowicz-Mehler, N., Fisk, R. A., Bennett, K., Gialeli-Goudas, M., Chew, P. W., Lau, J., Carr, D., & Americal Pain Society. (2003). Management of opioid side effects in cancer-related and chronic noncancer pain: A systematic review. *The Journal of Pain*, *4*, 231–256. https://doi.org/10.1016/S1526-5900(03)00556-X

Mogil, J. S. (2009). Animal models of pain: Progress and challenges. *Nature Reviews. Neuroscience*, *10*, 283–294. https://doi.org/10.1038/nrn2606

Nuckols, T. K., Anderson, L., Popescu, I., Diamant, A. L., Doyle, B., Di Capua, P., & Chou, R. (2014). Opioid prescribing: A systematic review and critical appraisal of guidelines for chronic pain. *Annals of Internal Medicine*, *160*, 38–47. https://doi.org/10.7326/0003-4819-160-1-201401070-00732

Patton, W. P., Chakravarthy, U., Davies, R. J., & Archer, D. B. (1999). Comet assay of UV-induced DNA damage in retinal pigment epithelial cells. *Investigative Ophthalmology & Visual Science*, *40*, 3268–3275.

Percie du Sert, N., Hurst, V., Ahluwalia, A., Alam, S., Avey, M. T., Baker, M., Browne, W. J., Clark, A., Cuthill, I. C., Dirnagl, U., Emerson, M., Garner, P., Holgate, S. T., Howells, D. W., Karp, N. A., Lazic, S. E., Lidster, K., Maccallum, C. J., Macleod, M., … Würbel, H. (2020). The ARRIVE guidelines 2.0: Updated guidelines for reporting animal research. *PLoS Biology*, *18*(7), e3000410. https://doi.org/10.1371/journal.pbio.3000410

Samaha, A. N., & Robinson, T. E. (2005). Why does the rapid delivery of drugs to the brain promote addiction? *Trends in Pharmacological Sciences*, *26*, 82–87.

Seven, I., Weinrich, T., Gränz, M., Grünewald, C., Brüß, S., Krstić, I., Prisner, T. F., Heckel, A., & Göbel, M. W. (2014). Photolabile protecting groups for nitroxide spin labels. *European Journal of Organic Chemistry*, *19*, 4037–4043.

Taura, J., Nolen, E. G., Cabré, G., Hernando, J., Squarcialupi, L., López-Cano, M., Jacobson, K. A., Fernández-Dueñas, V., & Ciruela, F. (2018). Remote control of movement disorders using a photoactive adenosine a 2A receptor antagonist. *Journal of Controlled Release*, *283*, 135–142. https://doi.org/10.1016/j.jconrel.2018.05.033

Tulleuda, A., Cokic, B., Callejo, G., Saiani, B., Serra, J., & Gasull, X. (2011). TRESK channel contribution to nociceptive sensory neurons excitability: Modulation by nerve injury. *Molecular Pain*, *7*, 30.

Urquhart, L. (2018). Market watch: Top drugs and companies by sales in 2017. *Nature Reviews. Drug Discovery*, *17*(4), 232. https://doi.org/10.1038/nrd.2018.42

Usoskin, D., Furlan, A., Islam, S., Abdo, H., Lönnerberg, P., Lou, D., Hjerling-Leffler, J., Haeggström, J., Kharchenko, O., Kharchenko, P. V., Linnarsson, S., & Ernfors, P. (2015). Unbiased classification of sensory neuron types by large-scale single-cell RNA sequencing. *Nature Neuroscience*, *18*, 145–153. https://doi.org/10.1038/nn.3881

Vargas-Schaffer, G., & Cogan, J. (2014). Patient therapeutic education: Placing the patient at the Centre of the WHO analgesic ladder. *Canadian Family Physician*, *60*, 235–241.

Velema, W. A., Szymanski, W., & Feringa, B. L. (2014). Photopharmacology: Beyond proof of principle. *Journal of the American Chemical Society*, *136*, 2178–2191. https://doi.org/10.1021/ja413063e

Volkow, N. D., & Thomas McLellan, A. (2016). Opioid abuse in chronic pain-misconceptions and mitigation strategies. *The New England Journal of Medicine*, *374*, 1253–1263. https://doi.org/10.1056/NEJMra1507771

Wegener, M., Hansen, M. J., Driessen, A. J. M., Szymanski, W., & Feringa, B. L. (2017). Photocontrol of antibacterial activity: Shifting from UV to red light activation. *Journal of the American Chemical Society*, *139*, 17979–17986. https://doi.org/10.1021/jacs.7b09281

Wong, P. T., Roberts, E. W., Tang, S., Mukherjee, J., Cannon, J., Nip, A. J., Corbin, K., Krummel, M. F., & Choi, S. K. (2017). Control of an unusual photo-Claisen rearrangement in Coumarin caged tamoxifen through an extended spacer. *ACS Chemical Biology*, *12*, 1001–1010. https://doi.org/10.1021/acschembio.6b00999

SUPPORTING INFORMATION

Additional supporting information may be found in the online version of the article at the publisher's website.

How to cite this article: López-Cano, M., Font, J., Aso, E., Sahlholm, K., Cabré, G., Giraldo, J., De Koninck, Y., Hernando, J., Llebaria, A., Fernández-Dueñas, V., & Ciruela, F. (2021). Remote local photoactivation of morphine produces analgesia without opioid-related adverse effects. *British Journal of Pharmacology*, 1–17. https://doi.org/10.1111/bph.15645